Generalised formulation of composite filters and their application to earthquake engineering test systems

David Paul Stoten*,†

Advanced Control and Test Laboratory (ACTLab), Department of Mechanical Engineering, University of Bristol, Bristol, BS8 1TR, UK

SUMMARY

This paper addresses the problem of generating unmeasured kinetic data - and/or providing improvements in existing data - for the enhancement of performance characteristics of earthquake engineering test systems, such as shaking tables, reaction walls and other custom-made test rigs. The approach relies upon the use of composite filters (CF), a method of data fusion that was originally conceived via transfer function formulation. The current work generalises the CF concept and extends its formulation into the state-space domain, thereby providing a wider basis for application to test systems and their controllers, including those of a multivariable (coupled, multi-axis) nature.

Comparative simulation studies of shaking table control are presented that demonstrate the design techniques for state-space CF and also their effectiveness for signal synthesis, noise suppression and performance improvement. Specific examples include the use of CF for displacement demand signal generation, velocity feedback generation and acceleration control. In each case, the essential principles behind CF – output signals with zero bias and zero drift – are consistently upheld.

KEY WORDS: composite filters, advanced testing, automatic control.

1. INTRODUCTION

The concept of composite filters (CF), a form of data fusion, was originally developed in order to generate real-time estimates of kinetic data, e.g. a velocity estimate based upon the fusion of two or more sources of congruent kinetic data such as acceleration and displacement signals; [1]. This former work was largely motivated by practical problems encountered within the field of earthquake engineering and the control of experiments using shaking tables, reaction walls and other forms of bespoke servohydraulically-actuated test rigs. In particular the generation of accurate, relatively noise-free feedback signals for test system controllers was a significant problem that was successfully addressed by the CF technique. A typical example was the generation of unmeasured velocity data using acceleration and displacement transducer signals, in order to improve the control of test rig transient performance characteristics.

A set of 10 CF was originally developed in [1], each member being named according to the types of input/output data; see the first column of Table I in Section 2.2 of the current paper. For example, the *ad2v* CF uses acceleration and displacement input data to generate an estimate of velocity as its output. Each filter is still required to satisfy the following conditions (rephrased from the original):

(i) Each CF consists of 2 or 3 parallel paths, with one CF element in each path - itself consisting of one auxiliary and one complementary filter component in series; see Section 2.2, Figure 1.

(ii) Each auxiliary filter component has a pure derivative or integral form, which is serially combined with its respective complementary filter component to produce a proper (or strictly proper) CF element.

*Correspondence to: David Paul Stoten, ACTLab, Department of Mechanical Engineering, University of Bristol, University Walk, Bristol BS8 1TR, UK.
†E-mail: d.p.stoten@bristol.ac.uk

(iii) For a given CF, the resultant gain and phase generated by the sum of its complementary filters are unity and zero, respectively.
(iv) Input signals to the CF can have non-zero means.
(v) Successive integration of input signals must be executed in a manner that ensures potential output bias and drift are removed after a suitably short transient period.
(vi) In general, high-derivative inputs are filtered by high-pass CF elements, intermediate-derivative inputs by intermediate-pass CF elements and low-derivative inputs by low-pass CF elements.
(vii) All CF elements are proper, or strictly proper, and of minimal order.

(Note that two logically feasible filters, *av2d* and *vd2a*, were absent from the original set of ten, because their formulations did not satisfy one or more of the conditions (i)-(vii)).

The subject matter of this current paper focuses on newly identified areas of investigation that are directly associated with the original signal synthesis and control work. The first of these areas is a generalisation of the CF concept, via a CF realisation within the state-space domain. The second is generation of control system displacement demand data from pre-recorded acceleration data, where such demand data is not otherwise readily available. The third is acceleration control of test rigs by making use of robust, wide-bandwidth *displacement* control strategies; this is referred to as indirect acceleration control. Therefore, the main objectives of the current paper are stated as follows:

(I) To improve the CF transfer function formulation in terms of consistency, order and structural symmetry.
(II) To translate the CF transfer function formulation into the state-space domain, thereby extending the range of applicability to general (control) systems and enhancing the associated analysis and synthesis techniques.
(III) To provide specific examples of using the new CF method within the field of earthquake engineering and, in particular, to demonstrate CF effectiveness in the following applications: (a) demand and feedback signal generation, (b) acceleration control and (c) adaptive control.

It is noted that these objectives are primarily associated with the use of CF for signal synthesis, signal noise suppression and data fusion for advanced test systems such as shaking tables. Hence, examples of shaking table control strategies are presented solely to illustrate the effectiveness of the CF themselves, rather than to investigate the effectiveness of associated control systems.

The rest of this paper is structured as follows. Section 2 presents the development of a consistent and generalised transfer function model for all 10 CF, from which a state-space model is determined, thus satisfying objectives (I) and (II). Sections 3 and 4 address objective (III) by presenting specific examples of applying the CF state-space format to earthquake engineering test systems and Section 5 summarises the main conclusions from this work.

2. GENERALISATION OF TRANSFER FUNCTION AND STATE-SPACE FORMS

This section addresses objectives (I) and (II). First of all, a continuous-time transfer function model of order n and relative degree 0 is presented in Section 2.1, thereby establishing a generalised representation for all CF in this work. Second, the model is transformed into the state-space domain; in Section 2.2 the minimal order required for a consistent CF formulation is determined as $n = 3$, so that the results of Section 2.1 are used to generate the ten 3-state CF descriptions that satisfy objective (I).

(Analysis is primarily conducted in the Laplace domain. For the sake of compactness, arguments involving the complex frequency and time, s and t, are omitted unless clarity demands their presence).

2.1 Transformation of a proper n^{th}-order transfer function into an equivalent state-space form

Consider a proper n^{th}-order transfer function, G, with input u and output y

$$\frac{y}{u} = G = \frac{\sum_0^n b_i s^i}{\sum_0^n a_i s^i}, \tag{1}$$

where $\{a_i, b_i\}$ are n^{th}-order denominator and numerator polynomial coefficients and, without loss of generality, the denominator polynomial is monic, ($a_n = 1$). Re-writing (1) in affine form, where the second term on the right-hand side of (2) has a structure that is strictly proper with unit relative degree:

$$G = b_n + \frac{\sum_0^{n-1} (b_i - b_n a_i) s^i}{\sum_0^n a_i s^i}. \tag{2}$$

Hence the output $y = y_1 + y_2$, where

$$y_1 = b_n u \; ; \quad y_2 = \frac{\sum_0^{n-1} (b_i - b_n a_i) s^i}{\sum_0^n a_i s^i} u \, . \tag{3}$$

From the second equation in (3)

$$y_2 = \sum_0^{n-1} \underbrace{[(b_i - b_n a_i)u - a_i y_2]}_{z_i} s^{i-n} = \sum_0^{n-1} \left(z_i / s^{n-i} \right), \tag{4}$$

which can be expanded as the following set of n nested integrals

$$y_2 = \frac{1}{s}(z_{n-1} + \cdots + \frac{1}{s}(z_1 + \frac{1}{s}(z_0))). \tag{5}$$

Now assign $y_2 = x_1$ and denote the successive integrands within (5) as sx_j. Then, by starting with the outermost integrand ($j = 1$) and progressing to the innermost ($j = n$), the state derivatives are given by:

$$sx_j = \begin{Bmatrix} z_{n-j} + x_{j+1} ; & j = 1, 2, ..., n-1 \\ z_0 \qquad\quad ; & j = n \end{Bmatrix}. \tag{6}$$

Therefore the required state-space representation is

$$\left.\begin{gathered} sx = Ax + Bu \, ; \quad y = Cx + Du; \\ \text{where } A = \begin{bmatrix} -a_{n-1} & 1 & 0 & \cdots & \cdots & 0 \\ -a_{n-2} & 0 & 1 & 0 & \cdots & 0 \\ \vdots & & & \ddots & & \\ \vdots & & & & \ddots & \\ a_1 & 0 & \cdots & \cdots & 0 & 1 \\ a_0 & 0 & \cdots & \cdots & \cdots & 0 \end{bmatrix}; \; B = \begin{bmatrix} b_{n-1} - b_n a_{n-1} \\ b_{n-2} - b_n a_{n-2} \\ \vdots \\ \vdots \\ b_1 - b_n a_1 \\ b_0 - b_n a_0 \end{bmatrix}; \; C^T = \begin{bmatrix} 1 \\ 0 \\ \vdots \\ \vdots \\ \vdots \\ 0 \end{bmatrix}; \; D = \begin{bmatrix} b_n \end{bmatrix} \end{gathered}\right\} \tag{7}$$

and $x = [x_1 \quad x_2 \quad \cdots \quad x_n]^T$.

2.2 Synthesis of specific 3rd-order filters in transfer function and state-space form

With a slight revision of the notation within [1], the proposed CF structure is as shown in Figure 1.

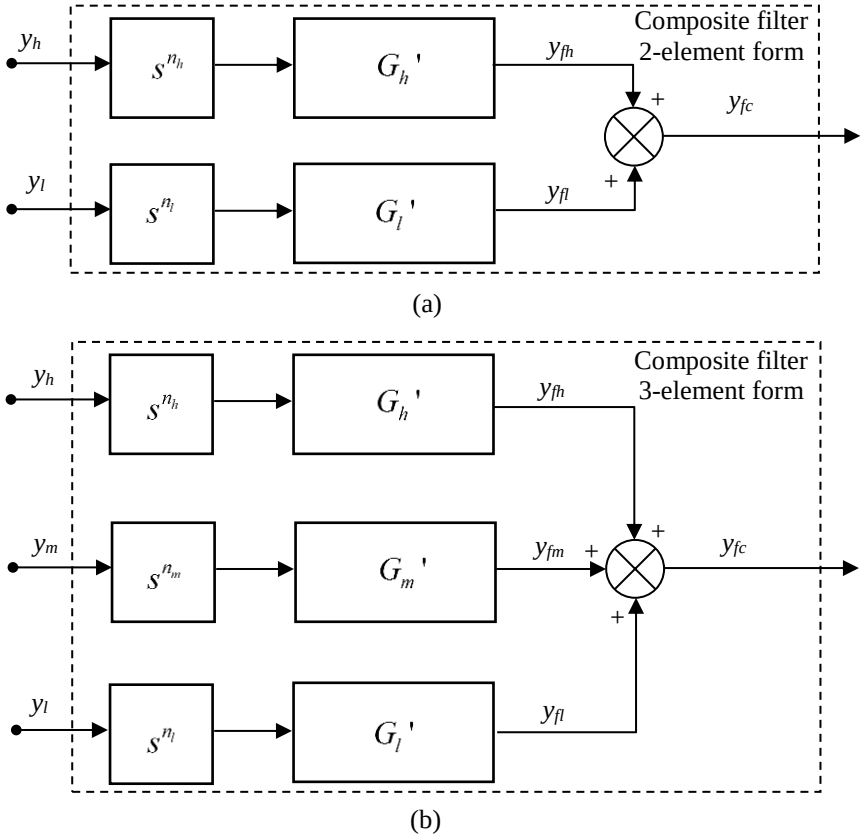

Fig. 1 Composite filters for kinetic data, showing their auxiliary (s^{n_p}) and complementary filter (G_p') components: (a) 2-element form; (b) 3-element form.

The figure shows that each CF element is comprised of two serial components: an auxiliary filter of the form s^{n_p}, where n_p determines the required number of differentiations or integrations, together with a complementary filter, G_p'. Each element is therefore described by $G_p = s^{n_p} G_p'$, which is combined with its companions in one of two ways: a 2-element form and a 3-element form. The 2-element CF shown in Figure 1(a) is driven by the pair of signals $\{y_h, y_l\}$, where the subscripts *h* and *l* refer to the highest and lowest derivative data, respectively. The output is a composite signal, y_{fc}, which is a filtered estimate of a given input signal or a congruent unmeasured signal. Thus, in the case of a 2-element CF, the complementary components are required to satisfy

$$G_h' + G_l' = 1. \tag{8}$$

Similarly for the 3-element CF shown in Figure 1(b), the input signals are $\{y_h, y_m, y_l\}$, where the subscript *m* refers to intermediate derivative data. Therefore, in this case

$$G_h' + G_m' + G_l' = 1. \tag{9}$$

A generalisation of the original CF development in [1] is to restrict all complementary filters to be of the same minimum order that also ensures satisfaction of conditions (i)-(vii) in Section 1. In [1] it was found that the corresponding minimum order could be $n = 2$ or 3, depending upon the CF; hence, the order is now fixed as $n = 3$ for all CF. Accordingly, the sum of terms on the left-hand side of both (8) and (9) is required to be equal to a 3rd-order monic transfer function defined by:

$$\left.\begin{array}{c} G_h' + G_l' \\ \text{or } G_h' + G_m' + G_l' \end{array}\right\} = \frac{s^3 + a_2 s^2 + a_1 s + a_0}{s^3 + a_2 s^2 + a_1 s + a_0}. \tag{10}$$

There is an arbitrary choice concerning the selection of the (stable) filter coefficients a_i and the partitioning of the numerator polynomial in the formulation of the complementary components. In order to address this issue an optimal H_∞-method of design was proposed in [2], based upon a choice of weighting functions derived from a knowledge of sensor noise and the underlying dynamics. In the current paper, straightforward use of Butterworth filters is continued from the earlier work, [1], requiring only an approximate estimate of a single break frequency, a, which is considered to be on the borderline between high and low frequency sensor signal data. In addition, numerator polynomials are partitioned in a manner that provides structural symmetry of the resulting CF formulation; comments on the sensitivity of varying the numerator structure are provided at the end of this sub-section. Thus, the 2-element CF complementary components are

$$G_h' = \frac{s^3 + a_2 s^2}{s^3 + a_2 s^2 + a_1 s + a_0};\ G_l' = \frac{a_1 s + a_0}{s^3 + a_2 s^2 + a_1 s + a_0} \tag{11}$$

and for the 3-element CF

$$G_h' = \frac{s^3}{s^3 + a_2 s^2 + a_1 s + a_0};\ G_m' = \frac{a_2 s^2 + a_1 s}{s^3 + a_2 s^2 + a_1 s + a_0};\ G_l' = \frac{a_0}{s^3 + a_2 s^2 + a_1 s + a_0}, \tag{12}$$

where the Butterworth coefficients are:

$$a_0 = a^3,\ a_1 = 2a^2,\ a_2 = 2a, \tag{13}$$

so that all CF elements, and hence the complete CF itself, have transient settling times approximated by [3]

$$t_s \approx 7 / a. \tag{14}$$

The numerators of the CF designs and the auxiliary filter indices are summarised in Table I, where all CF elemental denominators are given by the invariant polynomial ($s^3 + a_2 s^2 + a_1 s + a_0$).

Table I The set of 10 auxiliary filter indices and the CF elemental numerators.

CF name	Auxiliary filter indices			CF elemental numerators		
	n_h	n_m	n_l	G_h	G_m	G_l
ad2d	-2	-	0	$s+a_2$	-	$a_1 s+a_0$
ad2v	-1	-	+1	$s^2+a_2 s$	-	$a_1 s^2+a_0 s$
ad2a	0	-	+2	$s^3+a_2 s^2$	-	$a_1 s^3+a_0 s^2$
av2v	-1	-	0	$s^2+a_2 s$	-	$a_1 s+a_0$
av2a	0	-	+1	$s^3+a_2 s^2$	-	$a_1 s^2+a_0 s$
vd2d	-1	-	0	$s^2+a_2 s$	-	$a_1 s+a_0$
vd2v	0	-	+1	$s^3+a_2 s^2$	-	$a_1 s^2+a_0 s$
avd2d	-2	-1	0	s	$a_2 s+ a_1$	a_0
avd2v	-1	0	+1	s^2	$a_2 s^2+ a_1 s$	$a_0 s$
avd2a	0	+1	+2	s^3	$a_2 s^3+ a_1 s^2$	$a_0 s^2$

From the main result in Section 2.1, it is a straightforward matter to determine the equivalent state-space representation for each elemental numerator given in Table I. Thus, the corresponding elemental 'numerator' pairs $\{B_p, D_p\}$ are presented in Table II. Since the denominator polynomial is invariant for all CF, the corresponding 'denominator' pair in the state-space domain, $\{A, C\}$, is also invariant:

$$A = \begin{bmatrix} -a_2 & 1 & 0 \\ -a_1 & 0 & 1 \\ -a_0 & 0 & 0 \end{bmatrix};\ C = \begin{bmatrix} 1 & 0 & 0 \end{bmatrix}$$

Table II The set of 10 CF elemental 'numerator' pairs $\{B_p, D_p\}$; the 'denominator' pair $\{A, C\}$ is invariant for all CF.

CF name	CF elemental 'numerator' pairs $\{B_p, D_p\}$					
	B_h^T	D_h	B_m^T	D_m	B_l^T	D_l
ad2d	$[0\ \ 1\ \ a_2]$	[0]	-		$[0\ \ a_1\ \ a_0]$	[0]
ad2v	$[1\ \ a_2\ \ 0]$	[0]	-		$[a_1\ \ a_0\ \ 0]$	[0]
ad2a	$[0\ \ -a_1\ \ -a_0]$	[1]	-		$[a_0\text{-}a_1a_2\ \ -a_1^2\ \ -a_1a_0]$	$[a_1]$
av2v	$[1\ \ a_2\ \ 0]$	[0]	-		$[0\ \ a_1\ \ a_0]$	[0]
av2a	$[0\ \ -a_1\ \ -a_0]$	[1]	-		$[a_1\ \ a_0\ \ 0]$	[0]
vd2d	$[1\ \ a_2\ \ 0]$	[0]	-		$[0\ \ a_1\ \ a_0]$	[0]
vd2v	$[0\ \ -a_1\ \ -a_0]$	[1]	-		$[a_1\ \ a_0\ \ 0]$	[0]
avd2d	$[0\ \ 1\ \ 0]$	[0]	$[0\ \ a_2\ \ a_1]$	[0]	$[0\ \ 0\ \ a_0]$	[0]
avd2v	$[1\ \ 0\ \ 0]$	[0]	$[a_2\ \ a_1\ \ 0]$	[0]	$[0\ \ a_0\ \ 0]$	[0]
avd2a	$[-a_2\ \ -a_1\ \ -a_0]$	[1]	$[a_1\text{-}a_2^2\ \ -a_2a_1\ \ -a_2a_0]$	$[a_2]$	$[a_0\ \ 0\ \ 0]$	[0]

An example of *ad2v* CF design is presented in order to investigate the accuracy of unmeasured velocity estimation and to demonstrate the low sensitivity of changes to the numerator polynomial partitioning. Three cases are considered, yielding the following CF $\{B_p, D_p\}$ pairs, where case (2) corresponds to the symmetric partitioning design given in Tables I and II:

(1) G_h: s^2; G_l: $a_2s^3+ a_1s^2+ a_0$; $B_h^T = [1\ \ 0\ \ 0]$; $D_h = [0]$; $B_l^T = [a_1\text{-}\ a_2^2\ \ a_0\text{-}a_2a_1\ \ -a_2a_0]$; $D_l = [a_2]$

(2) G_h: s^2+a_2s; G_l: $a_1s^2+ a_0s$; $B_h^T = [1\ \ a_2\ \ 0]$; $D_h = [0]$; $B_l^T = [a_1\ \ a_0\ \ 0]$; $D_l = [0]$

(3) G_h: $s^2+a_2s+ a_1$; G_l: a_0s; $B_h^T = [1\ \ a_2\ \ a_1]$; $D_h = [0]$; $B_l^T = [0\ \ a_0\ \ 0]$; $D_l = [0]$

Input signals to the filter are taken from the 11th March 2011, Great East Japan earthquake acceleration and displacement data, $\{y_a, y_d\}$. Selecting a = 10 rad/s, Figure 2(a) confirms that the CF output from case (2), y_{vc2}, closely matches the actual velocity, y_v. After an initial transient period $t_s \approx 7/a = 0.7$ s, Figure 2(b) demonstrates that typical differences between the CF responses due to numerator partitioning, i.e. $y_{vc2} - y_{vc1}$ and $y_{vc2} - y_{vc3}$, are only ~2% of the velocity signal amplitude.

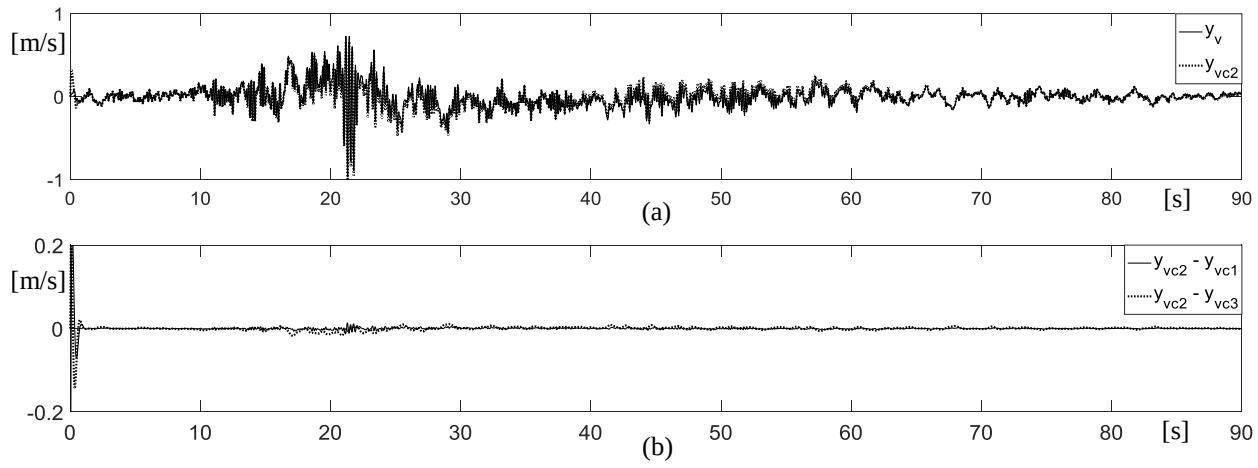

Fig. 2 *ad2v* CF performance when a = 10 rad/s: (a) Actual velocity signal and the nominal case (2) CF response, y_{vc2}; (b) Differences between the CF responses due to changes in numerator partitioning.

3. APPLICATION TO DEMAND GENERATION AND ACCELERATION CONTROL

The main purpose of this section is to address objective (III) by demonstrating the effectiveness of the CF state-space design by way of examples. Three commonly occurring problems in shaking table tests are investigated: (i) generation of control system displacement demand data, when only acceleration demand data are available, (ii) formulation of a well-conditioned indirect acceleration control strategy and (iii) generation of unmeasured velocity signals. Consequently, the focus will be on the design and use of the *ad2d* and *ad2v* CF. Single-axis problems are investigated for (i)-(iii),

although the methods of data filtering and control are equally applicable to coupled multi-axis (multivariable) systems; see further comments on this issue in Section 3.2.

3.1 Control system demand signal generation

Sole use of the high-pass element of *ad2d* can generate control system displacement demand data from a given acceleration record. In this case it is desirable that the break frequency, a, is set as low as possible in order to achieve a nearly pure, unbiased double-integration of the acceleration signal. However, the break frequency should not be too low, so that a reasonable transient time can also be achieved. For example, on selecting $a = 0.2$ rad/s (14) yields a transient time $t_s \approx 35$ s, which is acceptable, given that the range of the Tohoku earthquake data is 90 s. From Table 2, the corresponding demand signal filter is determined by $\{A, B_h, C, D_h\}$, where:

$$A = \begin{bmatrix} -0.4 & 1 & 0 \\ -0.08 & 0 & 1 \\ -0.008 & 0 & 0 \end{bmatrix};\ B_h = \begin{bmatrix} 0 \\ 1 \\ 0.4 \end{bmatrix};\ C = \begin{bmatrix} 1 & 0 & 0 \end{bmatrix};\ D_h = \begin{bmatrix} 0 \end{bmatrix}. \tag{15}$$

The zero mean acceleration input signal to the filter, y_a, is shown in Figure 3(a), whilst the resulting CF output, y_{dc}, is compared with a pure doubly-integrated acceleration signal, y_{ai2}, in Figure 3(b). As expected, y_{ai2} exhibits unacceptable drift, whereas y_{dc} is eminently suitable as a control system displacement demand when using a table with a maximum stroke of about ±1.0 m. An increase in a would reduce the stroke requirement, but also decrease the demanded displacement accuracy. Figure 3(c) provides further affirmation of the method, where application of the Welch method [4] to the doubly-differentiated displacement demand and the original acceleration signals shows their power spectral densities (PSD), P.d^2y_{dc} and P.y_a, to be virtually identical.

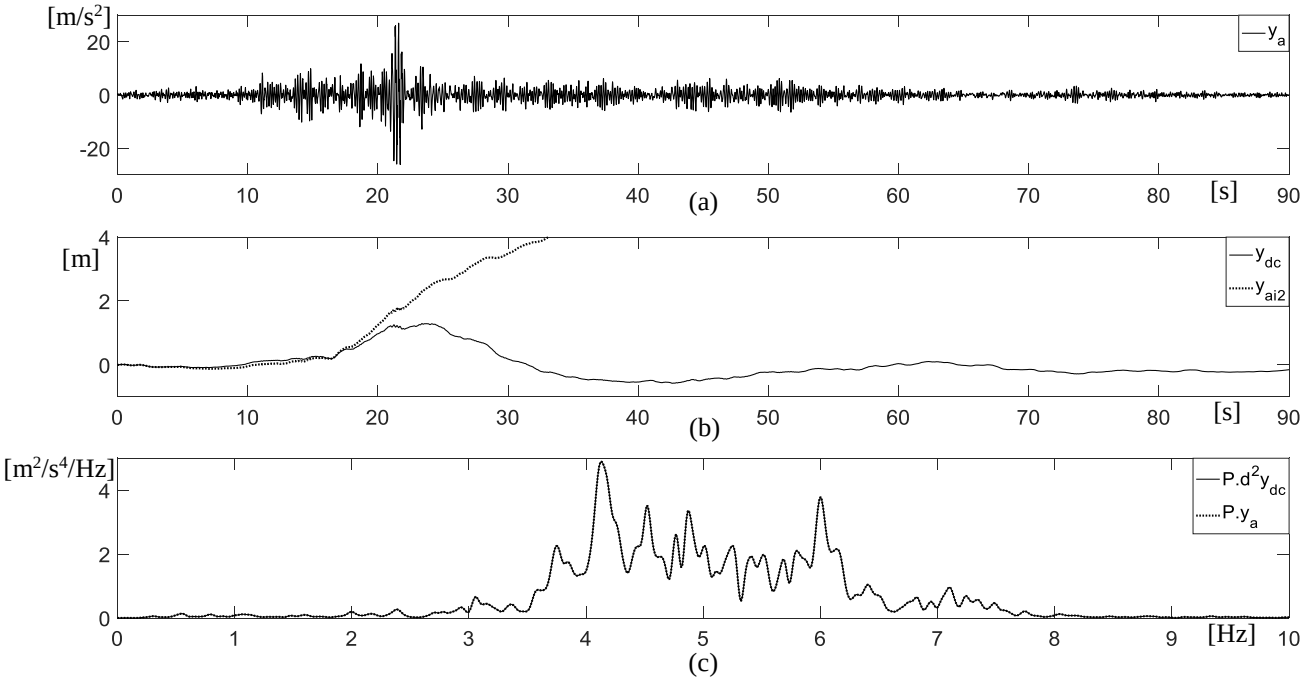

Fig. 3 High pass *ad2d* CF performance when $a = 0.2$ rad/s: (a) Great East Japan earthquake acceleration data, y_a; (b) CF output displacement signal, y_{dc}, and the doubly-integrated acceleration signal, y_{ai2}; (c) Welch method PSD of the doubly-differentiated filter output, P.d^2y_{dc}, and the original acceleration signal, P.y_a.

3.2 An indirect acceleration control strategy for shaking tables, with velocity signal estimation

Given that pre-recorded acceleration data are the main source of demand signals for shaking tables (and other test rigs within the field of earthquake engineering), the use of direct acceleration control (DAC) is a tempting proposition. One advantage of DAC is that it allows good fidelity of signal

resolution at high frequencies, compared with (say) the resolution provided by a conventional displacement control strategy. However DAC tends to result in unsatisfactory control at low frequencies and, unless suitable compensation is provided, unstable drift of unconstrained test machines will be an inevitable consequence. Examples of modified DAC strategies, which incorporate methods of circumventing the low frequency control and drift problems, include: high fidelity adaptive control [5], acceleration feedforward control with displacement feedback via Kalman filter estimation [6], control augmentation via force feedback [7] and feedforward control with multi-metric feedback [8]. Many of these and similar methods tend to rely upon a relatively complex mix of feedforward and feedback acceleration control, together with additional feedback of the displacement signal to overcome the problem of drift.

In contrast, the proposed method of indirect acceleration control (IAC) relies upon the concept of CF for the synthesis of a relatively straightforward and effective wide-bandwidth shaking table acceleration controller, founded upon a *displacement* control strategy. The general concept, shown in Figure 4 for a single-input, single-output (SISO) case, uses three physical signals: demanded acceleration, r_a, measured displacement, y_d, and measured acceleration, y_a. Hence the demanded acceleration, r_a, is processed either on-line or off-line by the high pass element of *ad2d*, with its break frequency, a_l, set to a relatively low value; cf. Section 3.1. The resulting output, r_d, then constitutes the displacement demand to the closed-loop controller, which is also supplied by the two wide-bandwidth composite feedback signals of shaking table displacement, y_{dc}, and velocity, y_{vc}. In turn, y_{dc} and y_{vc} are the signals generated by the feedback filters *ad2d* and *ad2v*, each being fed by the relatively narrow-bandwidth sensor measurements of displacement, y_d, and acceleration, y_a. Both *ad2d* and *ad2v* in the feedback loop have the same break frequency, a_h, set to an intermediate-to-high value; cf. Section 2. The IAC loop is completed by the generation of the displacement controller signal, u, being any suitably designed function of $\{r_d, y_{dc}, y_{vc}\}$.

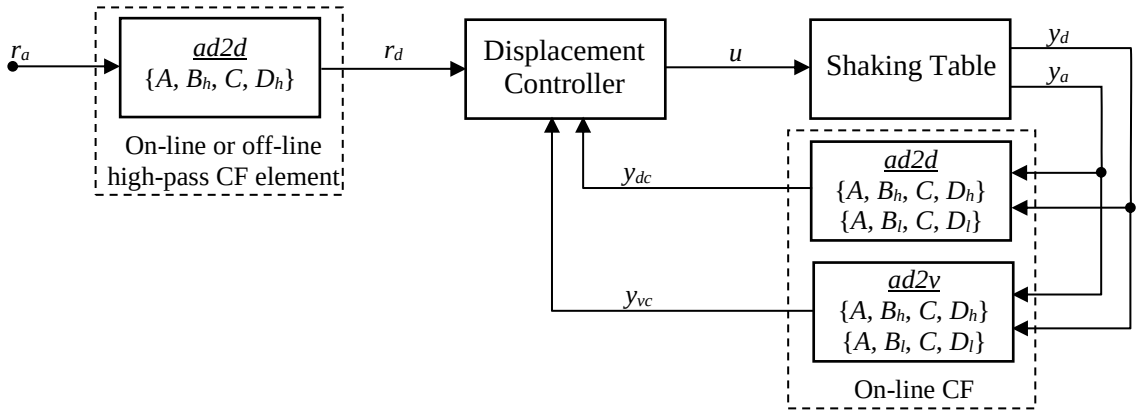

Fig. 4 Indirect acceleration control (IAC) of a shaking table using displacement control and CF.

Some notes on the IAC strategy follow:

- Closed-loop control is centred upon the use of a filtered displacement signal, y_{dc}. This results in the suppression of signal noise that is often problematic in DAC designs and, as a consequence, CF enable the use of high gain designs that yield controlled responses with high-fidelity.
- In addition, the filtered displacement signal, y_{dc}, has a wide-bandwidth content that is of crucial importance at higher frequencies, when displacement amplitudes are small. This attribute of CF further enhances control system fidelity and compares very favourably with a strategy that directly uses the relatively narrow-bandwidth sensor signal, y_d.
- The CF designs are independent of both the controller and the shaking table dynamic parameters, which is a significant advantage over alternative observer and Kalman filter-based methods.

- Similarly, the controller design is independent of the CFs, since each CF in the feedback loop is based upon the use of complementary filters that have unit gain and zero phase over the entire frequency spectrum. In principal, any stabilising controller strategy can be used, for example SISO, multi-input/multi-output (MIMO), fixed-gain and adaptive strategies can all be adopted within the IAC configuration. Extension to the $m > 1$ degree-of-freedom (DOF) MIMO case is straightforward: with reference to Figure 4, each DOF will have its own forward loop CF for the generation of r_{di} and a pair of feedback loop CF for the generation of y_{dci} and y_{vci}, $i = 1, 2, \ldots, m$. The design of each CF will therefore remain independent of the MIMO system dynamics, including any coupling effects.
- Figure 4 arbitrarily shows two feedback loops, y_{dc} and y_{vc}. However, depending upon the requirements of the control system design, the number of feedback loops could be one (y_{dc}), two (y_{dc} and y_{vc}, or y_{dc} and y_{ac}) or three (y_{dc}, y_{vc} and y_{ac}).

As an illustrative example, Figure 5(a) shows the IAC configuration of a basic SISO proportional-derivative (PD) controller with gains k_p and k_d, utilising an *ad2d* (a = 100 rad/s) CF in the feedback loop. This is fed by acceleration and displacement outputs from the shaking table, together with a high-pass *ad2d* (a = 0.2 rad/s) CF element in the feedforward loop. An alternative state feedback controller (SFC) with gain $K_e = [K_{e1} \quad K_{e2}]$, suitable for application to both SISO and MIMO shaking tables, is shown in Figure 5(b). Here, it is assumed that each DOF is adequately modelled by two states, displacement and velocity, so that parallel *ad2d* and *ad2v* CF are used in the feedback loop to construct the state as $x_c = [y_{dc} \quad y_{vc}]^T$. Correspondingly, the feedforward loop contains parallel high-pass *ad2d* and *ad2v* CF elements to generate the reference vector $x_r = [r_d \quad r_v]^T$.

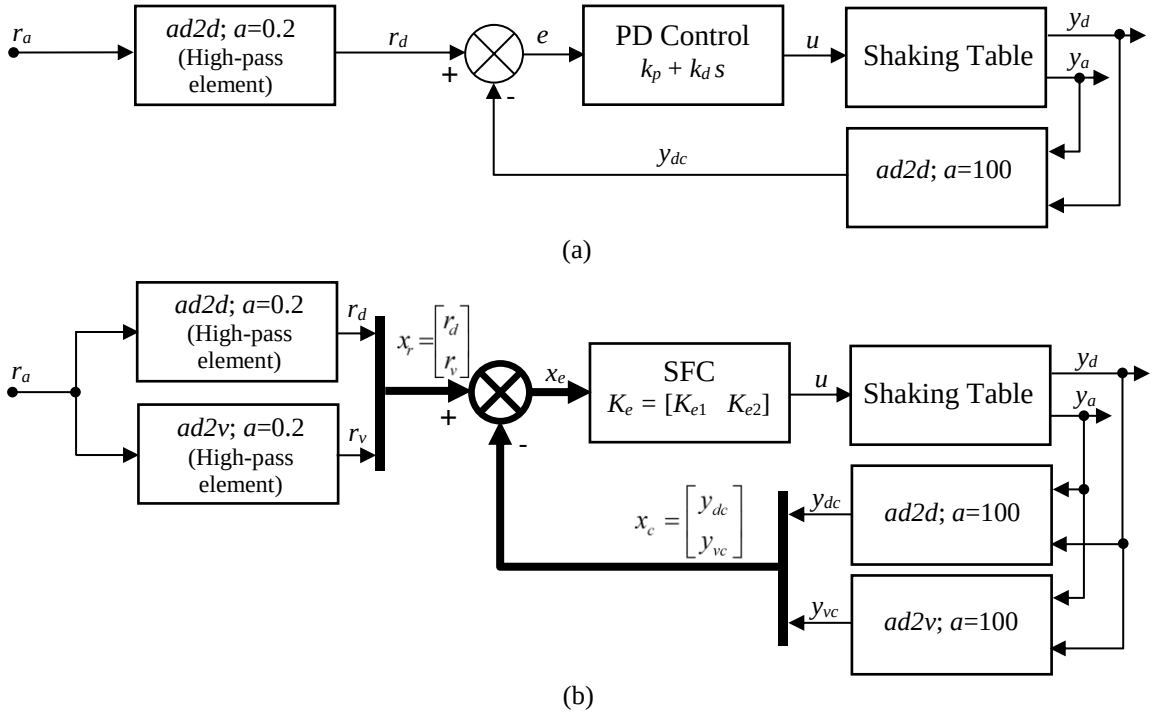

Fig. 5 Two examples of CF-based shaking table IAC: (a) Proportional-derivative control; (b) State feedback control.

The performance of a typical SISO IAC that incorporates SFC is now examined via a numerical example, with the following motivation: (i) to demonstrate the effectiveness of the CF within a closed-loop configuration and (ii) to show that high-gain control is facilitated via the noise suppression effects of CF in the feedback and feedforward loops. For the sake of simplicity, the following SISO 2-state linear model of an unconstrained shaking table is adopted:

$$sx_p = A_p x_p + B_p u; \quad \text{where } A_p = \begin{bmatrix} 0 & 1 \\ 0 & -c/m \end{bmatrix} = \begin{bmatrix} 0 & 1 \\ 0 & -0.1 \end{bmatrix}; \; B_p = \begin{bmatrix} 0 \\ k_m/m \end{bmatrix} = \begin{bmatrix} 0 \\ 10 \end{bmatrix}$$

and the state vector, x_p, consists of the table displacement and velocity, c = 1000 Ns/m is the table viscous friction coefficient, $m = 10^4$ kg is the table mass and $k_m = 10^5$ N/V is the table actuator drive constant. Drive system dynamics are considered to be of a much higher bandwidth than those of the table and are ignored here. CF are designed using Table II, with values of break frequency, a, as shown in Figure 5(b). The design for the SFC gain is K_e = [1000 20], ensuring a closed-loop error response with critical damping and a natural frequency of ~100 rad/s. In addition, measurement noise is superimposed upon both the displacement (y_d) and acceleration (y_a) signals in the system of Figure 5(b), each contributing an uncorrelated ~0.1 m/s^2 root-mean-square component to y_a.

A basic form of SFC was initially investigated in order to provide a benchmark for judging the effectiveness of the CF. Here, the direct measurement of y_d was used in place of y_{dc} in Figure 5(b), together with a velocity estimate, y_v, in place of y_{vc}. The velocity estimate was formed via approximate differentiation of y_d, thus: $y_v(s) = [s/(0.01s+1)]y_d(s)$. The resulting responses are shown in Figure 6, where the peak acceleration and displacement errors are, respectively, ~13 m/s^2 in Figure 6(a) and ~2.2×10^{-3} m in Figure 6(b). There is also noticeable error between the acceleration reference and response PSDs up to ~30 Hz, as shown in Figure 6(c). Figure 6(d) shows the acceleration root-integral-square-error (RISE) curve, a monotonically increasing measure of performance defined as $I_{raya} = \left[(1/t_f) \int_0^{t_f} (r_a - y_a)^2 \, dt \right]^{0.5}$, which attains a final value of ~1.08 m/s^2 at t_f = 90 s.

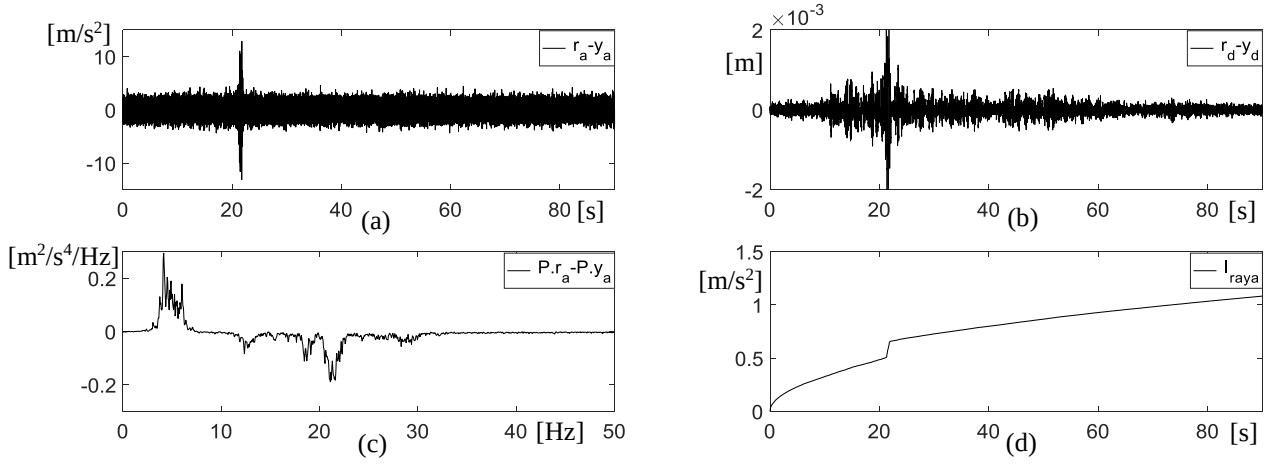

Fig. 6 Benchmark IAC shaking table SFC with a velocity filter: (a) Acceleration error r_a-y_a; (b) Displacement error r_d-y_d; (c) Acceleration PSD error P.r_a - P.y_a; (d) Acceleration RISE I_{raya}.

The comparative responses of the CF-based strategy of Figure 5(b) are shown in Figure 7, where the peak acceleration and displacement errors are, respectively, ~6.2 m/s^2 in Figure 7(a) and (again) ~2.2×10^{-3} m in Figure 7(b). Hence, the acceleration errors have been reduced by a factor of ~2. Noticeable errors between the acceleration reference and response PSDs now exist up to only ~12 Hz, as shown in Figure 7(c), whilst the RISE curve now attains a lower (i.e. better) value of ~0.391 m/s^2 at t_f = 90 s. This corresponds to an ~2.8-fold improvement in acceleration performance due to the action of the CF.

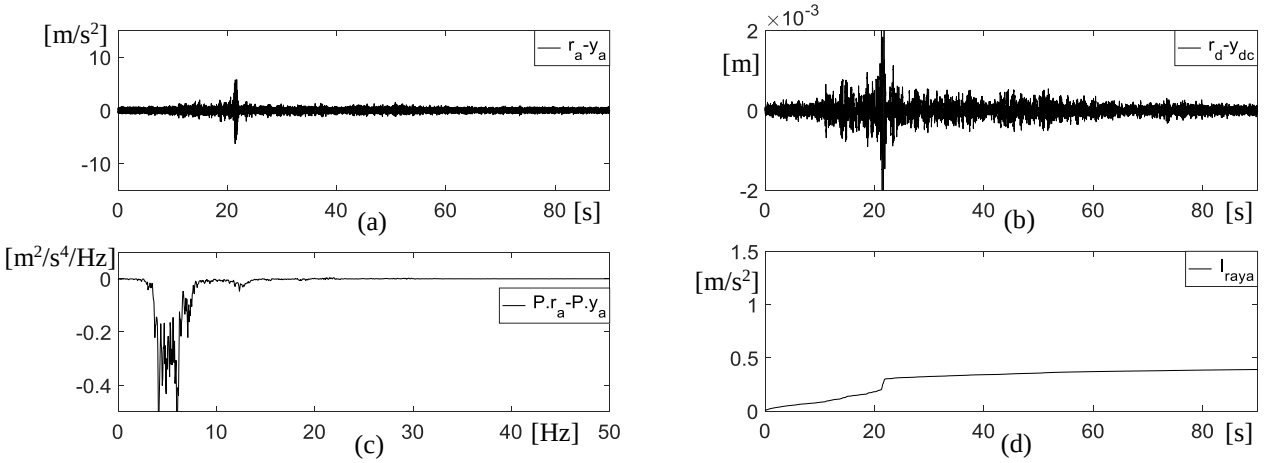

Fig. 7 CF-based IAC shaking table SFC: (a) Acceleration error r_a-y_a; (b) Displacement error r_d-y_{dc}; (c) Acceleration PSD error P.r_a - P.y_a; (d) Acceleration RISE I_{raya}.

Finally, it is noted that a CF-based indirect velocity control (IVC) strategy can also be synthesised in a very similar manner to the IAC strategy.

4. COMPOSITE FILTERS AND ADAPTIVE CONTROL OF SHAKING TABLES

Together with the Appendix, this section addresses the third objective, (III). Nonlinear adaptive algorithms belonging to the class labelled minimal control synthesis (MCS) have been successfully implemented as controllers for shaking tables since the 1990s, demonstrating high levels of tracking accuracy in the face of uncertain dynamic properties and disturbances; [5], [9], [10]. Detuned MCS algorithms tend to be used in practice, in order to prevent adaptive gain drift (windup) due to the deleterious effects of signal noise; [11]. The use of CFs proves to be particularly effective, since the filtering can enable high-gain adaption without the need for detuning and the consequential danger of induced gain drift leading to instability. Demonstration of this aspect of CF usage constitutes the main objective of this section.

An innovation to the MCS class is also introduced, labelled as the minimal control synthesis error algorithm (MCS-E). The most notable attributes of MCS-E, when compared with the original MCS algorithm, are that it has (i) a relatively simple structure that requires only n adaptive feedback gains (for each DOF), where n is the order of the plant dynamics and (ii) a significantly improved, automatic gain magnitude conditioning that is the result of being driven entirely by error signals. This section briefly presents the MCS-E algorithm, within the context of CF-based shaking table control, by continuation of the example from the previous section. Since this is the first formal presentation of MCS-E, a generalised proof of the algorithm's hyperstability [12] is included in the Appendix (although this is not essential reading, given the principle objectives of this paper).

With reference to Figure 8, the closed-loop configuration of the MCS-E algorithm, shaking-table and CFs is similar to that of the SFC in Figure 5(b). One significant difference is that the time-varying vector gain of the MCS-E algorithm, $K_e(t)$, is now determined via a continuous, adaptive process that is described in detail in the Appendix. Another difference is that the shaking table (i.e. plant) dynamic parameters, represented by the pair $\{A_p, B_p\}$, are generally assumed to be unknown and time-varying. The corresponding state vector, x_p, is constructed from the outputs of *ad2d* and *ad2v* in the feedback loop. In addition, an unknown and time-varying term, d, can act upon the plant, representing the effects of any external disturbances and internal parametric variations. When compared with Figure 5(b), the principal change in the forward loop is that no *ad2v*-generated estimate of the velocity demand is required. Instead, a reference model described by the fixed-parameter pair $\{A_m, B_m\}$ now uses the forward loop elemental *ad2d* output, $r = r_d$, to generate a modified and filtered form of the displacement and velocity demands, as represented by

the state x_m. Again, the previously described additive noise processes are assumed to corrupt both y_d and y_a.

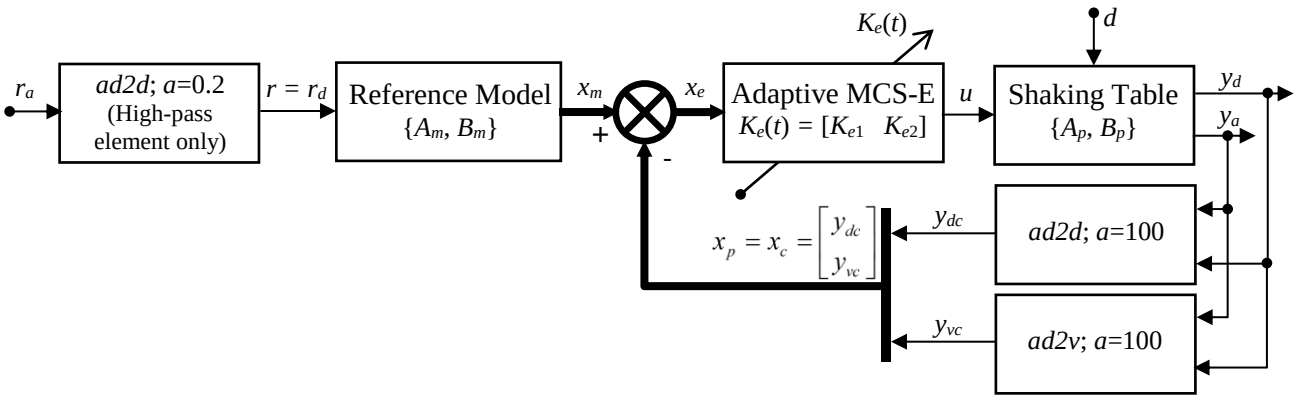

Fig. 8 Adaptive MCS-E control of a shaking table.

Apart from the choice of reference model parameters, the only other terms required for the design of MCS-E, as given in (A4), are two scalar adaptive weights α = 1000 and β = 100 – values that are usually determined by empirical means [5]. To demonstrate the effectiveness of CF, the shaking table control example of Section 3 is investigated further. In this case, knowledge of the plant parameters is not necessary, although a two-state reference model is required. This is designed to have a critically damped response, a natural frequency ω_n = 100 rad/s and a static gain of unity. As a consequence, the pair $\{A_m, B_m\}$ is given by

$$A_m = \begin{bmatrix} 0 & 1 \\ -a_{m1} & -a_{m2} \end{bmatrix};\ B_m = \begin{bmatrix} 0 \\ a_{m1} \end{bmatrix};\ a_{m1} = 10^4\,\mathrm{s}^{-2},\ a_{m2} = 200\,\mathrm{s}^{-1}, \tag{16}$$

As with the SFC policy of Section 3, a simple velocity filter can be used to generate an estimate of y_v from the displacement, y_d, and these two signals used in place of y_{vc} and y_{dc} in Figure 8. This provides a benchmark from which CF effectiveness can be evaluated, as shown by the responses in Figure 9. Particularly noticeable in this figure are the undesirable and continual growths in acceleration error amplitude (Figure 9(a)), the acceleration performance index (Figure 9(d)) and the controller gains (Figures 9(e), (f)). In addition, the velocity filter causes a deleterious effect on the acceleration PSD error, especially in the range 50-100Hz (Figure 9(c)). The unrestrained growth in controller gains is of particular concern, since this will usually result in instability with time.

Reverting to the use of CF within the MCS-E algorithm considerably improves this situation, as shown in Figure (10). Retaining the scales of axes used in Figure 9, it is seen that the previous growth problem associated with error amplitude, acceleration performance index and controller gains has been eliminated; see Figure 10(a),(d),(e),(f). In particular, despite the presence of signal noise, the use of CF has resulted in quasi-steady state values of 0.390 m/s^2, 3.04 V/m and 116 Vs/m for the acceleration performance index, displacement gain and velocity gain, respectively.

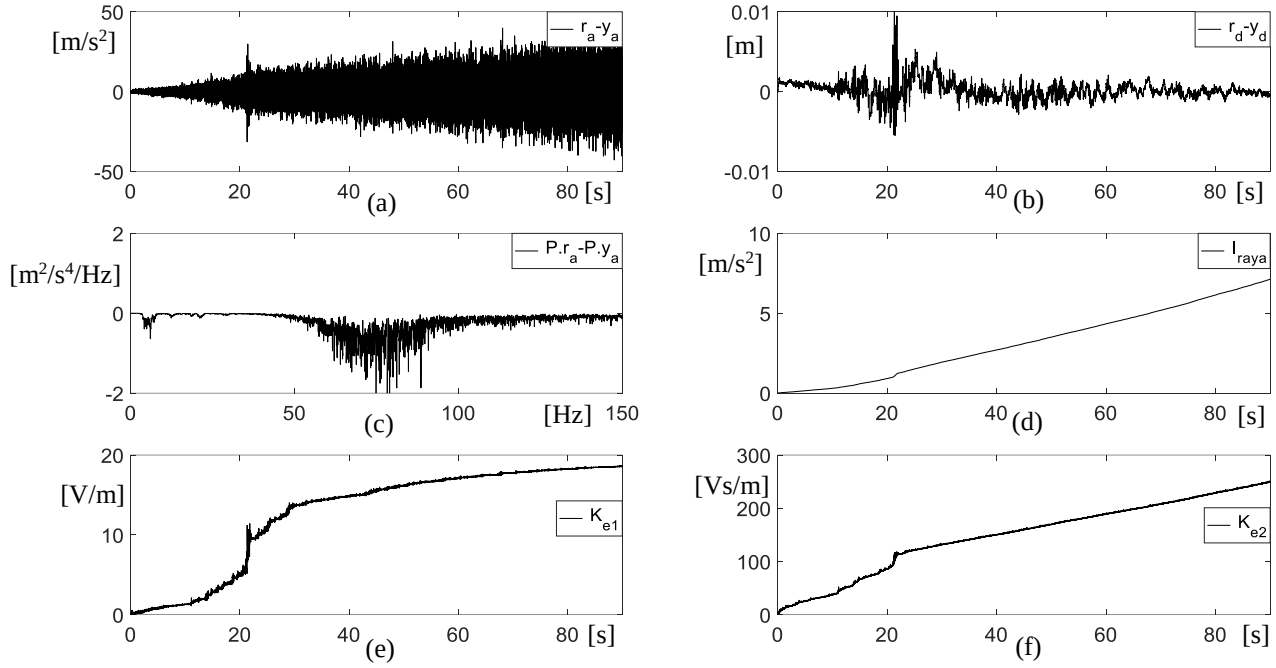

Fig. 9 IAC shaking table MCS-E with a velocity filter: (a) Acceleration error r_a-y_a; (b) Displacement error r_d-y_d; (c) Acceleration PSD error P.r_a - P.y_a; (d) Acceleration RISE I_{raya}; (e) Gain $K_{e1}(t)$; (f) Gain $K_{e2}(t)$.

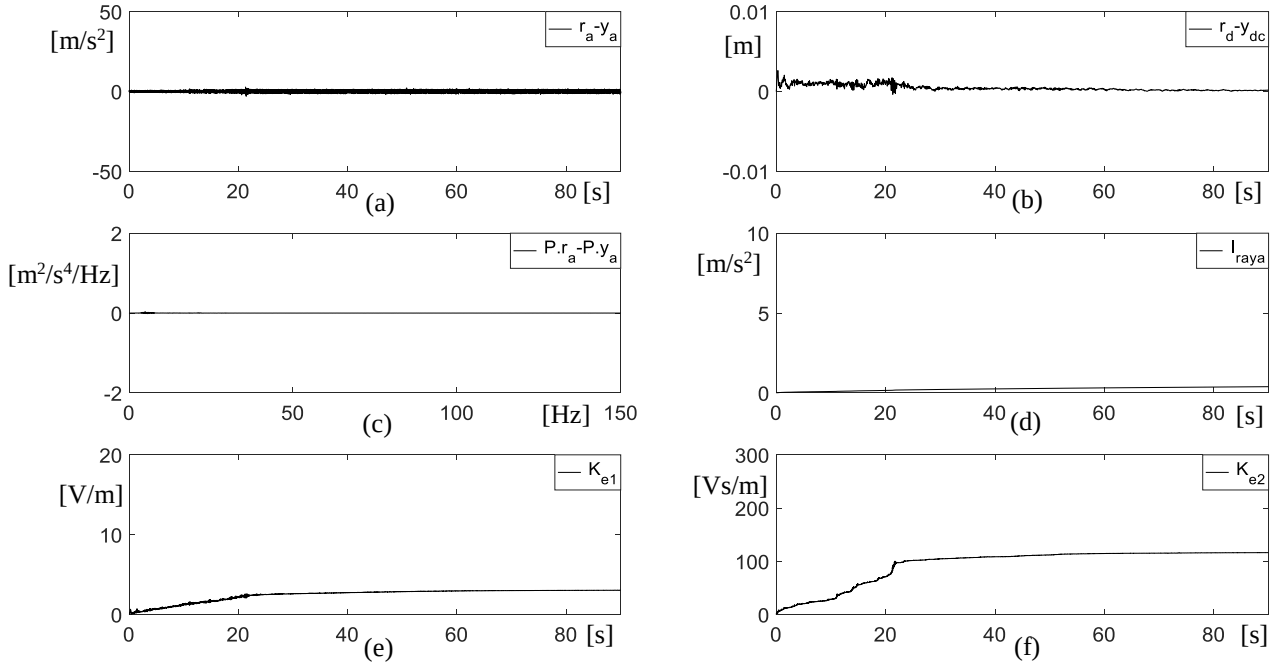

Fig. 10 CF-based IAC shaking table MCS-E: (a) Acceleration error r_a-y_a; (b) Displacement error r_d-y_{dc}; (c) Acceleration PSD error P.r_a - P.y_a; (d) Acceleration RISE I_{raya}; (e) Gain $K_{e1}(t)$; (f) Gain $K_{e2}(t)$.

5. CONCLUSIONS

The main conclusions to be drawn from this work are as follows:

(1) This paper is centred upon the further rationalisation and generalisation of an original concept for composite filters (CF), a form of data fusion, into the state-space domain. A set of 10 CF has been obtained. The paper describes how the new CF formulation can be used in a number of situations, with an emphasis on application to the control of shaking tables – a problem that clearly shows the beneficial properties of CF. However, this paper is not intended to be a

discourse on the state-of-the-art in shaking table control; the interested reader is directed to a recent review of this topic in [14].

(2) Each CF was a 3-state system represented by the parameter quadruple $\{A, B_p, C, D_p\}$, where $\{A, C\}$ was invariant and $\{B_p, D_p\}$ was dependent upon the specific CF.

(3) CF designs were based upon a single parameter, i.e. the break frequency, a, that defined the approximate boundary between individual sensor bandwidths. Therefore the designs were independent of the (controlled) system dynamics, irrespective of the number of degrees-of-freedom (DOF) and dynamic coupling between the DOF.

(4) The basic properties of CF - zero bias and zero drift in their output signals - were effectively used in a number of circumstances: demand signal generation, synthesis of unmeasured signals, noise filtering of measured signals and extension of sensor signal bandwidths.

(5) CF contain complementary filters that introduce unit gain and zero phase within a particular loop. Hence, a control system design can be performed quite separately from the CF design, and vice versa, for any given test system.

(6) A specific indirect acceleration control (IAC) strategy was presented that utilised the beneficial properties of CF in order to:

   (i) determine a zero-bias/zero-drift equivalent displacement demand from an original acceleration demand signal,

   (ii) enable a wide-bandwidth displacement controller to use the demand signal from (i), together with the CF-generated displacement/velocity feedback signals, and

   (iii) suppress the effects of measurement noise.

(7) A new form of adaptive control, the minimal control synthesis error algorithm (MCS-E), was also presented. MCS-E is tailored specifically for problems encountered in earthquake engineering test systems, potentially yielding very accurate responses even when parameter knowledge of the controlled system is poor. However, as with most other adaptive or self-tuning control algorithms, MCS-E by itself can be sensitive to signal noise – potentially causing problems in unrestrained parameter (gain) growth and possibly leading to instability. Again, the use of CF was shown to preserve the positive attributes of the adaptive algorithm, whilst completely suppressing any noise-driven gain windup.

ABBREVIATIONS

CF	composite filter
DAC	direct acceleration control
DOF	degree of freedom
IAC	indirect acceleration control
IVC	indirect velocity control
MCS	minimal control synthesis (algorithm)
MCS-E	minimal control synthesis error (algorithm)
MIMO	multi-input/multi-output
NL	nonlinear (system)
RISE	root integral square error
SFC	state feedback control
SISO	single-input/single-output
SPR	strictly positive real

REFERENCES

1. Stoten DP. Fusion of kinetic data using composite filters. *Proc. IMechE, Part I: J. Systems and Control Engineering*, 2001, **215**:63-79.
2. Plummer AR. Optimal complementary filters and their application in motion measurement. *Proc. IMechE, Part I: J. Systems and Control Engineering*, 2006, **220**:489-507.
3. D'Azzo JJ, Houpis CH. *Feedback Control System Analysis and Synthesis*, 1966, Kougakusha Co. Ltd, Tokyo.
4. Welch PD. The use of Fast Fourier Transform for the estimation of power spectra: A method based on time averaging over short, modified periodograms, *IEEE Transactions on Audio and Electroacoustics*, 1967, **15**(2):70-73.
5. Stoten DP, Gomez E. Adaptive control of shaking tables using the minimal control synthesis algorithm. *Phil. Trans. R. Soc. Lond.* A, 2001, **359**(1786):1697-1723.
6. Nakata N. Acceleration trajectory tracking control for earthquake simulators. *Engineering Structures*, 2010, **32**(8):2229-2236.
7. Stehman M, Nakata N. Direct acceleration feedback control of shake tables with force stabilization. *Journal of Earthquake Engineering,* 2013, **17**(5):736-749.
8. Phillips BM, Wierschem NE, Spencer Jr BF. Model-based multi-metric control of uniaxial shake tables. *Earthquake Engng Struct. Dyn.*, 2014, **43**:681-699.
9. Stoten DP, Gomez E. Recent application results of adaptive control on multi-axis shaking tables, *Seismic Design Practice into the Next Century*, 1998, AA Balkema publishers, (Rotterdam):381-387.
10. Gomez E, Stoten DP. A comparative study of the adaptive MCS control algorithm on European shaking tables, 2000, *12th World Congress on Earthquake Engineering*, Auckland, NZ.
11. Stoten DP. Investigation of an adaptive control algorithm incorporating anti-windup, anti-ratcheting protection, 2004, UK Automatic Control Conference (UKACC), University of Bath.
12. Popov VM. *Hyperstability of Control Systems*, 1973, Springer-Verlag, Berlin.
13. Landau YD. *Adaptive Control – The Model Reference Approach*, 1979, Marcel Dekker, New York.
14. Yao J, Dietz M, Xiao R, Yu H, Wang T, Yue D. An overview of control schemes for hydraulic shaking tables. *Journal of Vibration and Control*, 2016, **22**(12):1-17.

APPENDIX

The purpose of this section is to present a proof of MCS-E based system hyperstability, making use of the following four-step procedure:

Step 1: *Plant and reference model dynamics.* The n^{th}-order SISO plant dynamics are modelled by a state equation in phase canonical form, with state vector x_p and scalar (control) input u, where n is assumed to be known:

$$\dot{x}_p = A_p x_p + B_p u + d; \quad A_p = \begin{bmatrix} 0 & 1 & 0 & \cdots & \cdots & 0 \\ 0 & 0 & 1 & 0 & \cdots & 0 \\ & & & \ddots & & \\ & & & & \ddots & \\ 0 & \cdots & \cdots & \cdots & 0 & 1 \\ -a_{p1} & -a_{p2} & \cdots & \cdots & \cdots & -a_{pn} \end{bmatrix}; \quad B_p = \begin{bmatrix} 0 \\ \vdots \\ \vdots \\ \vdots \\ 0 \\ b_{p1} \end{bmatrix}; \quad d = \begin{bmatrix} 0 \\ \vdots \\ \vdots \\ \vdots \\ 0 \\ d_1 \end{bmatrix}. \quad \text{(A1)}$$

The plant parameters $\{a_{pi}, b_{p1}\}$ and the disturbance d_1 are unknown and time-varying although the sign of b_{p1} is assumed to be known, so that $b_{p1} > 0$ without loss of generality. In addition, the reference model has the same n^{th}-order phase-canonical structure as the plant, with state vector x_m and scalar (reference) input r. By design, all reference model parameters $\{a_{mi}, b_{m1}\}$ are known and

possibly time-varying, A_m is a Hurwitz matrix and very often $b_{m1} = a_{m1}$, so that the model possesses a static gain of unity:

$$\dot{x}_m = A_m x_m + B_m r; \quad A_m = \begin{bmatrix} 0 & 1 & 0 & \cdots & \cdots & 0 \\ 0 & 0 & 1 & 0 & \cdots & 0 \\ & & & \ddots & & \\ & & & & \ddots & \\ 0 & \cdots & \cdots & \cdots & 0 & 1 \\ -a_{m1} & -a_{m2} & \cdots & \cdots & \cdots & -a_{mn} \end{bmatrix}; \quad B_m = \begin{bmatrix} 0 \\ \vdots \\ \vdots \\ \vdots \\ 0 \\ b_{m1} \end{bmatrix}. \tag{A2}$$

Step 2: *Adaptive control law and the closed-loop error dynamics.* The nonlinear control law is structurally linear in u, whereby the time-varying adaptive gain $K_e(t)$ operates upon the state error, x_e, according to

$$u = K_e(t) x_e, \text{ where } \; x_e = x_m - x_p. \tag{A3}$$

With the time argument omitted from this point onwards, the proposed nonlinear 'proportional-integral' formulation of the $1 \times n$ adaptive gain is

$$\left.\begin{aligned} K_e &= \alpha \int_0^t y_e x_e^T \, d\tau + \beta y_e x_e^T; \; K_e(0) = 0 \\ K_e &= [K_{ei}]; \; K_{ei} = \alpha \int_0^t y_e x_{ei} \, d\tau + \beta y_e x_{ei} \end{aligned}\right\}, \tag{A4}$$

where $\{\alpha > 0, \beta \geq 0\}$ are scalar adaptive weights that can be selected according to an empirical method described in [5]. The output error term, y_e, is a linear function of the state error, x_e, and is described in more detail in the succeeding text. In practice, the zero initial condition on K_e in (A4) is guaranteed by assigning $x_m(0) = x_p(0)$. Significantly, (A4) indicates that each gain term K_{ei} is generated solely from the measurable signals $\{y_e, x_{ei}\}$ and the fixed scalar weights $\{\alpha, \beta\}$. From (A1)-(A3), the closed-loop system error dynamics can be written as

$$\dot{x}_e = A_m x_e + (A_p - A_m - B_p K_e) x_e + (A_m - A_p) x_m + B_m r - d \, . \tag{A5}$$

Due to the assumed phase-canonical formulations, (A5) can be re-written as

$$\dot{x}_e = A_m x_e + B_e [A_p - A_m - B_p K_e]_n x_e + B_e [(A_m - A_p) x_m + B_m r - d]_n, \tag{A6}$$

where $B_e^T = \begin{bmatrix} 0 & \cdots & 0 & 1 \end{bmatrix}$ and $[\cdots]_n$ defines the n^{th} row of the given matrix or vector. Collecting terms in (A6) yields

$$\dot{x}_e = A_m x_e + B_e \underbrace{([A_p - A_m - B_p K_e]_n + B_f^T)}_{\Phi} x_e, \tag{A7}$$

where the entries of $B_f^T = \begin{bmatrix} b_{f1} & \cdots & b_{fn} \end{bmatrix}$ are assumed to satisfy the existence condition $\sum_1^n b_{fi} x_{ei} = b_{m1} r - d_1 + \sum_1^n (a_{pi} - a_{mi}) x_{mi}$ for the non-trivial case $x_e \neq 0$.

The term $\Phi = ([A_p - A_m - B_p K_e]_n + B_f^T)$ in (A7) provides the final form of the error dynamics that is required at the core of the hyperstability analysis

$$\dot{x}_e = A_m x_e + B_e \Phi x_e \, . \tag{A8}$$

Equation (A8) implies that the error dynamics are globally asymptotically stable if the term Φx_e in the particular integral vanishes within a finite time.

Step 3: *Output error and visualisation of the error dynamics as a nonlinear regulator.* Regarding the output error, y_e, this signal is generated by the linear mapping

$$y_e = C_e x_e, \tag{A9}$$

where the output error matrix, C_e, is used in Step 4 to ensure satisfaction of the strictly positive real (SPR) condition that is central to this analysis. The combination of (A8) and (A9) can be visualised as the closed-loop regulator shown in Figure A1, where the forward loop triple $\{A_m, B_e, C_e\}$ represents an entirely known linear system, whilst the nonlinear feedback block, NL, describes the system unknowns and uncertainties within (A8).

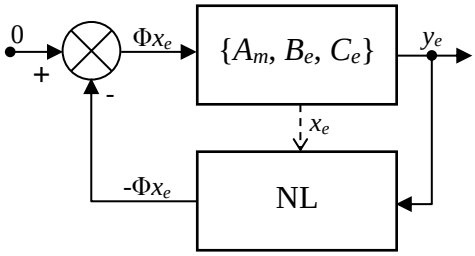

Fig. A1 Error dynamics structured as a regulator, with linear forward and nonlinear (NL) feedback blocks.

Step 4: *The Popov Criterion and proof of hyperstability.* Given the structure of Figure A1, hyperstability of the error dynamics is guaranteed if the triple $\{A_m, B_e, C_e\}$ is SPR and the NL block satisfies the Popov criterion, (A12), when applied to the input and output signals y_e and $-\Phi x_e$; [12], [13]. The SPR condition is investigated via the Kalman-Yakubovitch-Popov lemma, [13], by initially assigning

$$C_e = B_e^T P, \tag{A10}$$

so that $\{A_m, B_e, C_e\}$ is SPR when P is the positive definite symmetric solution to the Lyapunov equation

$$A_m^T P + P A_m = -Q \tag{A11}$$

for a given $Q > 0$. Then, the Popov criterion is given by the inequality; [12]

$$\Gamma = \int_{t_1}^{t_2} (y_e)(-\Phi x_e)\, dt \geq -\gamma^2 ; \ \forall t_2 \geq t_1, \tag{A12}$$

where Γ is the Popov integral and $-\gamma^2$ is a strictly negative, but an otherwise arbitrary scalar quantity. Decomposing $\Phi = [A_p - A_m - B_p K_e]_n + B_f^T$ into its constituent integral (α) and proportional (β) parts yields

$$\left.\begin{aligned} &\Phi = [\phi_i]; \ \ \phi_i = \phi_{\alpha i} + \phi_{\beta i} \\ &\phi_{\alpha i} = -a_{pi} + a_{mi} + b_{fi} - b_{p1}\alpha \int_0^t y_e x_{ei}\, d\tau \\ &\phi_{\beta i} = -b_1 \beta y_e x_{ei} \end{aligned}\right\}. \tag{A13}$$

Hence:

$$y_e x_{ei} = -\frac{\phi_{\beta i}}{b_{p1}\beta} \approx -\frac{\dot{\phi}_{\alpha i}}{b_{p1}\alpha}, \tag{A14}$$

where the approximation arises from the time derivative of the second equation within (A13), i.e. the bandwidth of variation in each term of the quadruple $\{a_{pi}, a_{mi}, b_{fi}, b_{p1}\}$ is assumed to be significantly less than that of the product of the errors, $y_e x_{ei}$. This is an intuitively reasonable

assumption, because each term in the product is a function of terms within the quadruple; therefore a bandwidth separation factor of at least two can be expected. Decomposing the Popov integral in a similar manner to Φ and making use of (A14) yields

$$\left.\begin{aligned} &\Gamma = \sum\nolimits_1^n \Gamma_i ; \quad \Gamma_i = \Gamma_{\alpha i} + \Gamma_{\beta i} \\ &\Gamma_{\alpha i} = \int_{t_1}^{t_2} -y_e \phi_{\alpha i} x_{ei}\, dt \\ &\Gamma_{\beta i} = \int_{t_1}^{t_2} -y_e \phi_{\beta i} x_{ei}\, dt \end{aligned}\right\}, \tag{A15}$$

where an equality is now assumed in place of the approximation within (A14).

Performing the integrations within (A15) results in the inequalities of (A16) and (A17)

$$\Gamma_{\alpha i} = \int_{t_1}^{t_2} \frac{\dot{\phi}_{\alpha i}\phi_{\alpha i}}{b_{p1}\alpha}\, dt = \frac{1}{2b_{p1}\alpha}\phi_{\alpha i}^2 \Bigg|_{t_1}^{t_2} \geq -\frac{1}{2b_{p1}\alpha}\phi_{\alpha i}^2(t_1) = -\gamma_{\alpha i}^2 , \tag{A16}$$

$$\Gamma_{\beta i} = \int_{t_1}^{t_2} \frac{1}{b_{p1}\beta}\phi_{\beta i}^2\, dt \geq 0 = -\gamma_{\beta i}^2 . \tag{A17}$$

Hence the reassembled integral, Γ, satisfies the Popov inequality (cf. A12):

$$\Gamma \geq -\sum\nolimits_1^n \gamma_{\alpha i}^2 = -\gamma^2 , \tag{A18}$$

which completes the proof of closed-loop hyperstability.

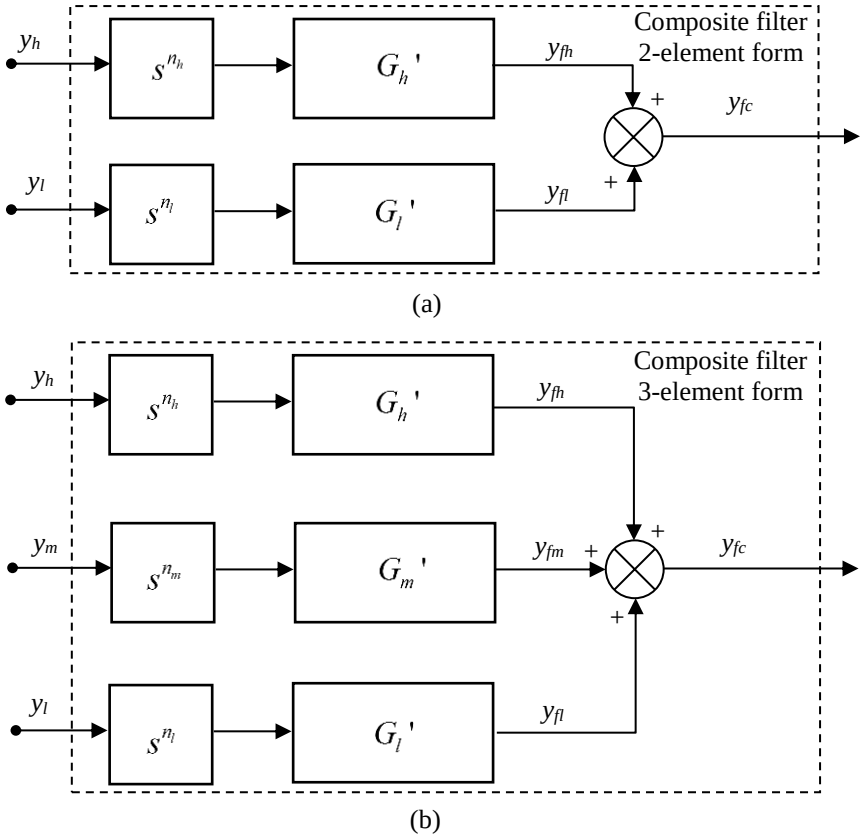

Fig. 1 Composite filters for kinetic data, showing their auxiliary (s^{n_p}) and complementary filter (G_p') components: (a) 2-element form; (b) 3-element form.

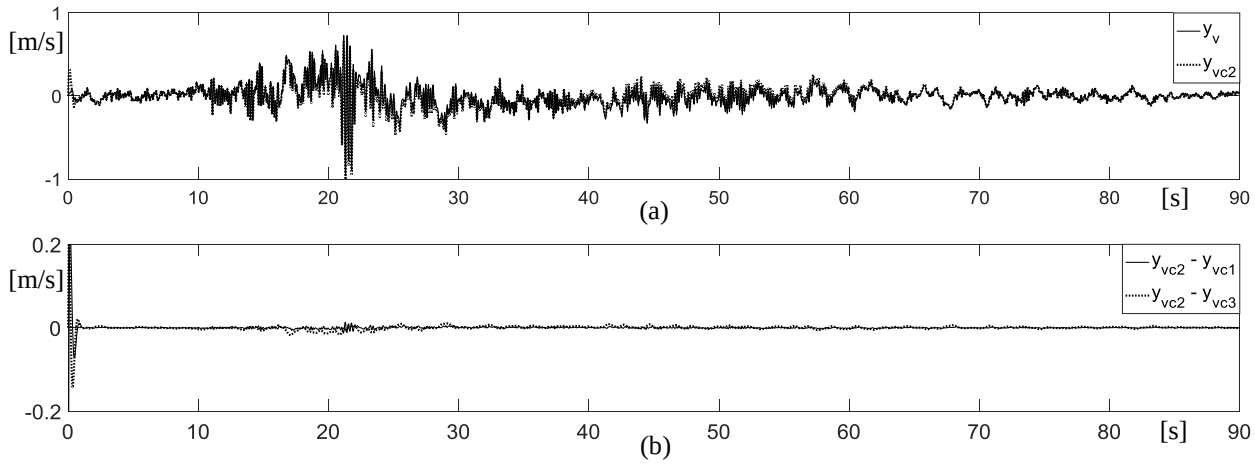

Fig. 2 *ad2v* CF performance when a = 10 rad/s: (a) Actual velocity signal and the nominal case (2) CF response, y_{vc2}; (b) Differences between the CF responses due to changes in numerator partitioning.

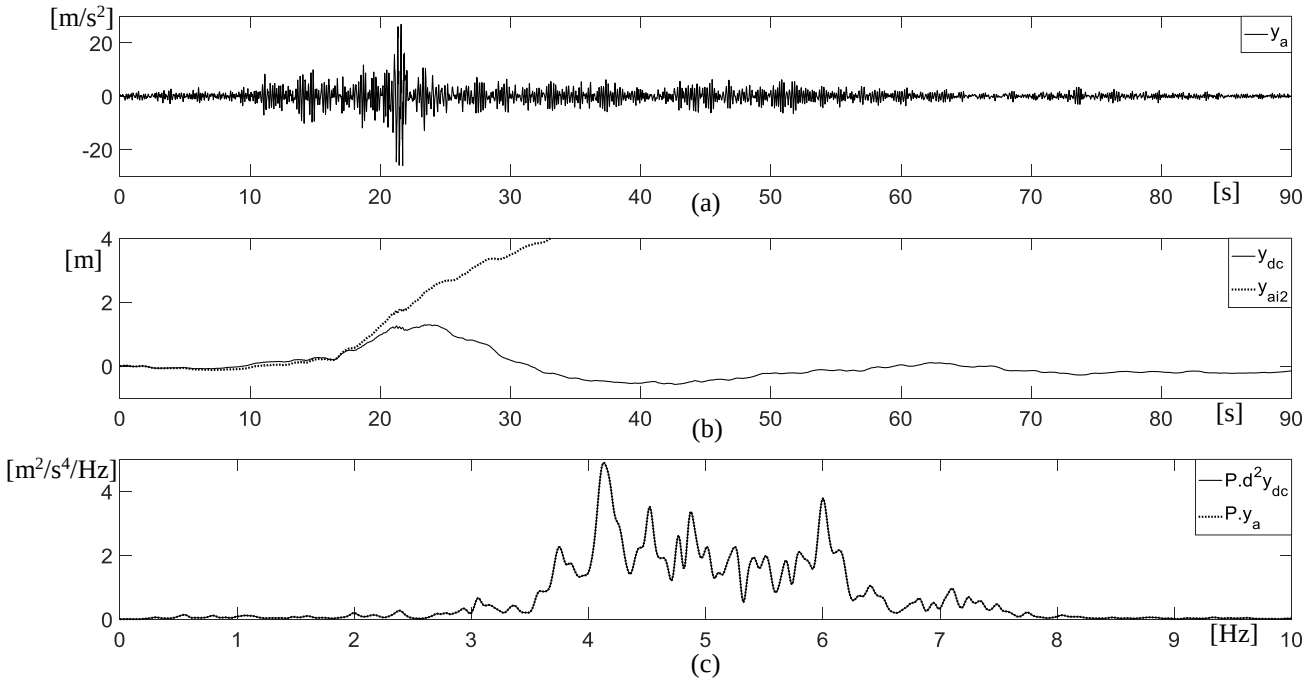

Fig. 3 High pass *ad2d* CF performance when a = 0.2 rad/s: (a) Great East Japan earthquake acceleration data, y_a; (b) CF output displacement signal, y_{dc}, and the doubly-integrated acceleration signal, y_{ai2}; (c) Welch method PSD of the doubly-differentiated filter output, P.d^2y_{dc}, and the original acceleration signal, P.y_a.

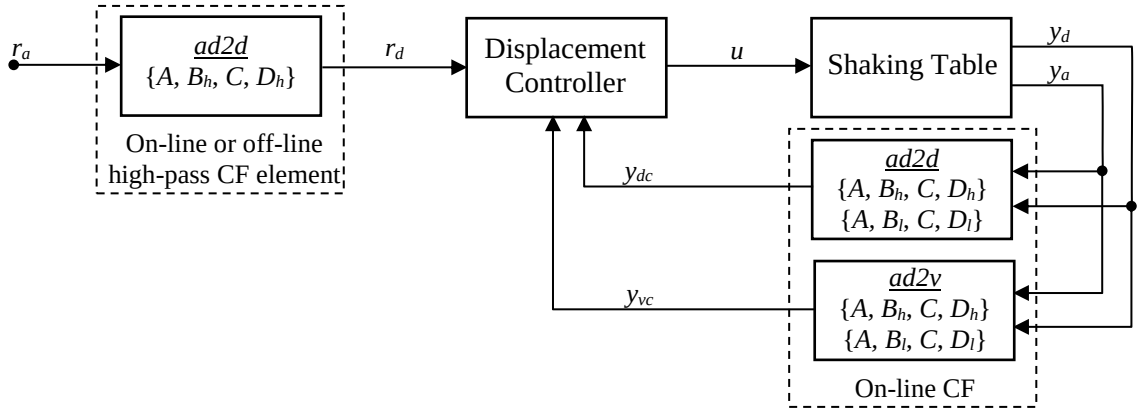

Fig. 4 Indirect acceleration control (IAC) of a shaking table using displacement control and CF.

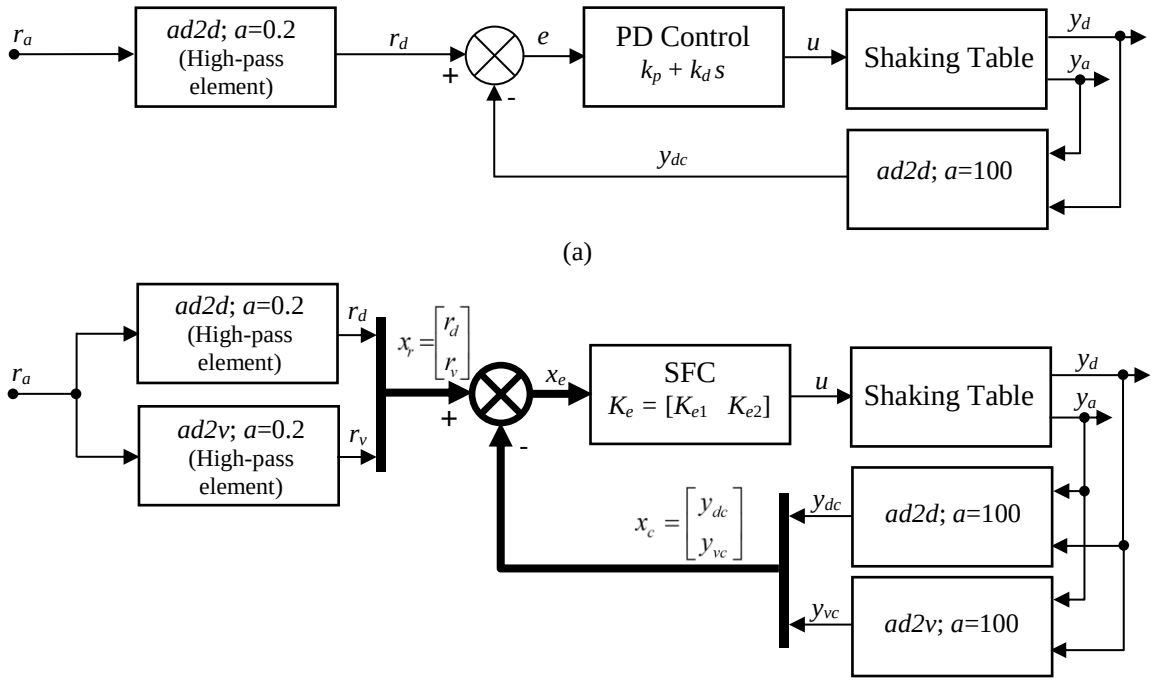

Fig. 5 Two examples of CF-based shaking table IAC: (a) Proportional-derivative control; (b) State feedback control.

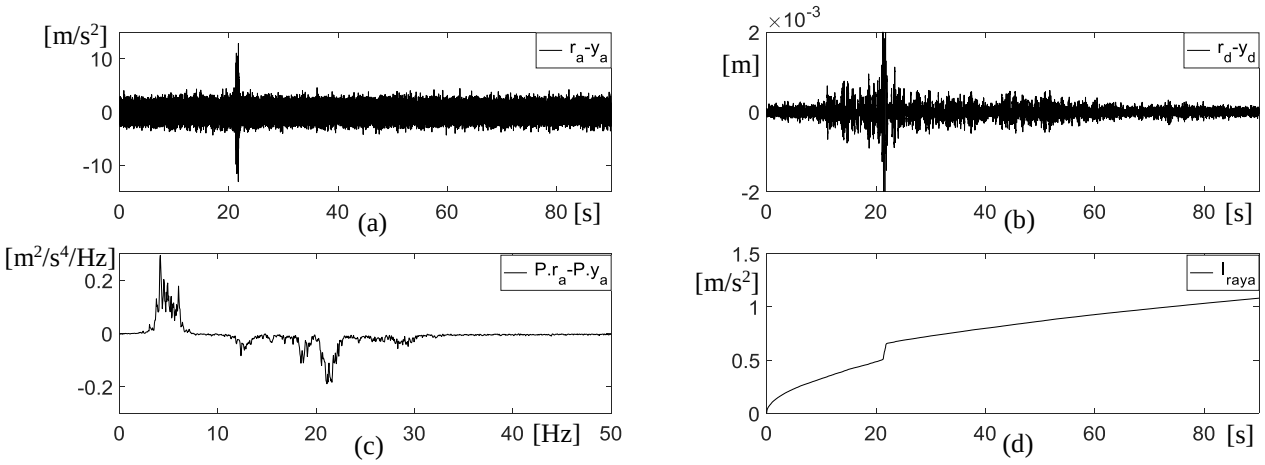

Fig. 6 Benchmark IAC shaking table SFC with a velocity filter: (a) Acceleration error r_a-y_a; (b) Displacement error r_d-y_d; (c) Acceleration PSD error P.r_a - P.y_a; (d) Acceleration RISE I_{raya}.

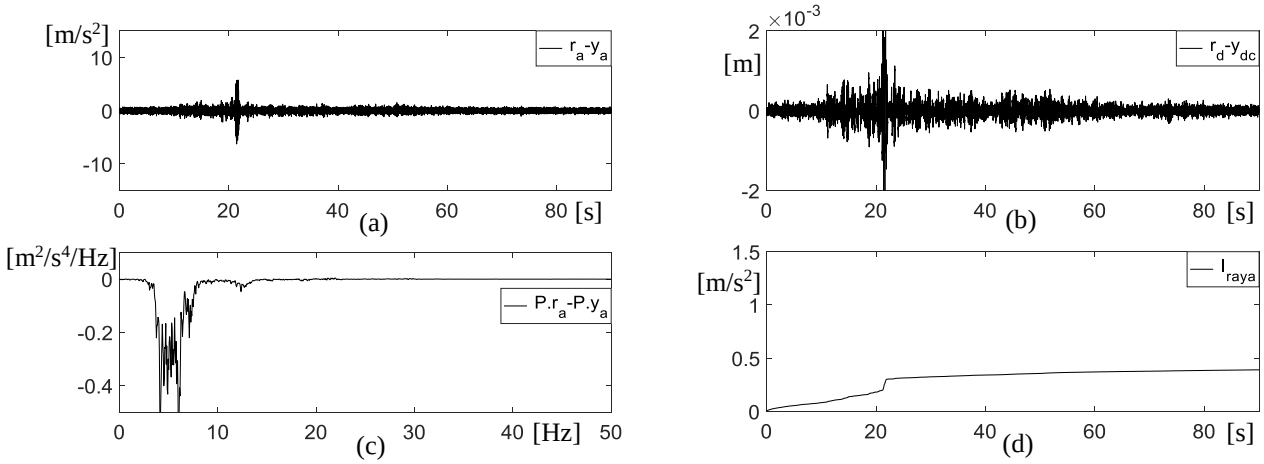

Fig. 7 CF-based IAC shaking table SFC: (a) Acceleration error r_a-y_a; (b) Displacement error r_d-y_{dc}; (c) Acceleration PSD error P.r_a - P.y_a; (d) Acceleration RISE I_{raya}.

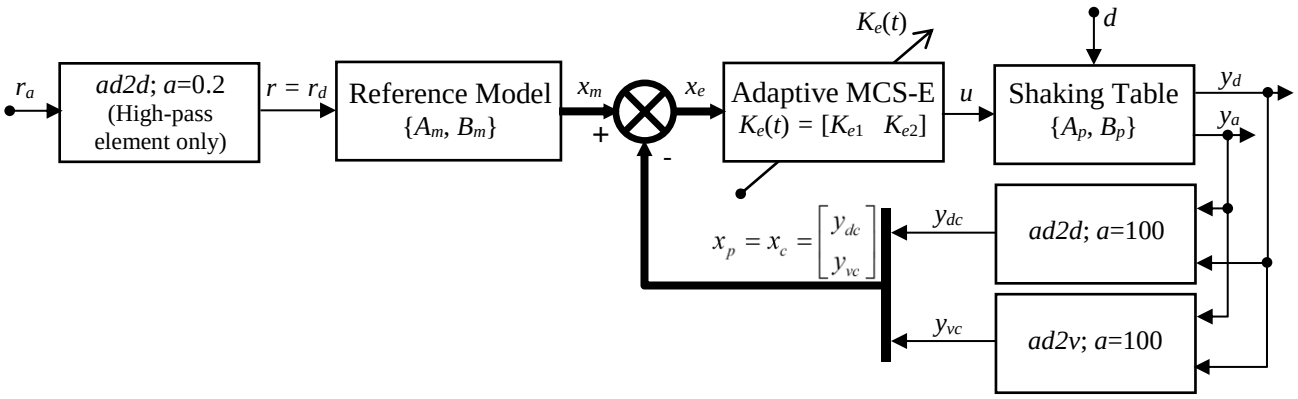

Fig. 8 Adaptive MCS-E control of a shaking table.

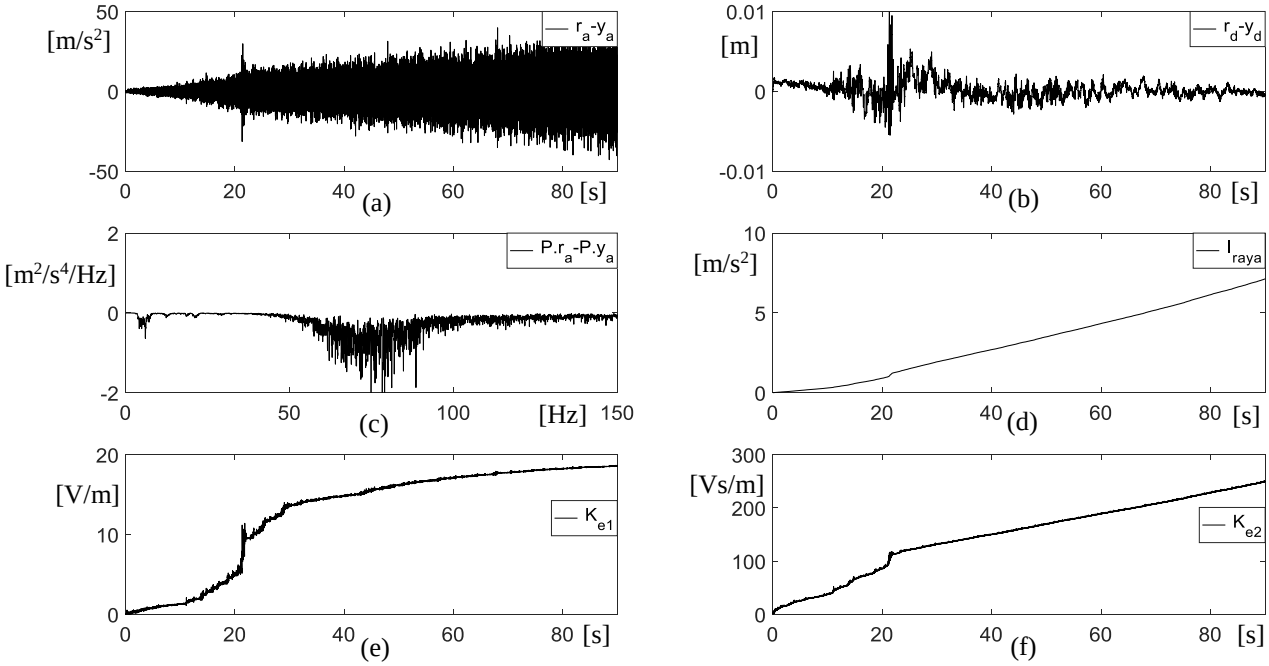

Fig. 9 IAC shaking table MCS-E with a velocity filter: (a) Acceleration error r_a-y_a; (b) Displacement error r_d-y_d; (c) Acceleration PSD error P.r_a - P.y_a; (d) Acceleration RISE I_{raya}; (e) Gain $K_{e1}(t)$; (f) Gain $K_{e2}(t)$.

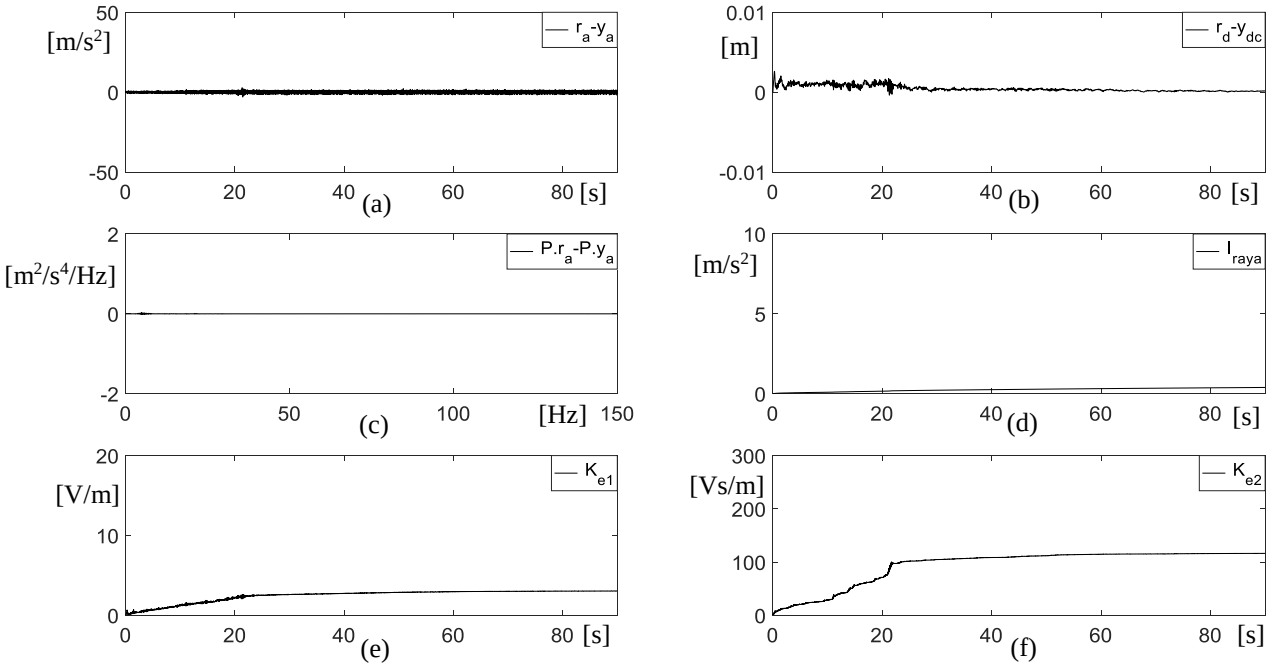

Fig. 10 CF-based IAC shaking table MCS-E: (a) Acceleration error r_a-y_a; (b) Displacement error r_d-y_{dc}; (c) Acceleration PSD error P.r_a - P.y_a; (d) Acceleration RISE I_{raya}; (e) Gain $K_{e1}(t)$; (f) Gain $K_{e2}(t)$.

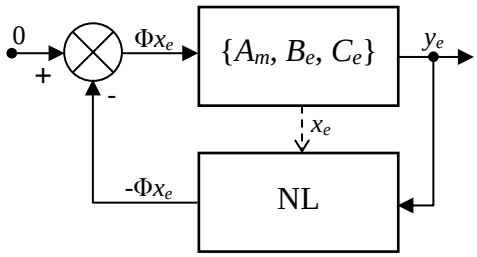

Fig. A1 Error dynamics structured as a regulator, with linear forward and nonlinear (NL) feedback blocks.

Table I The set of 10 auxiliary filter indices and the CF elemental numerators.

CF name	Auxiliary filter indices			CF elemental numerators		
	n_h	n_m	n_l	G_h	G_m	G_l
ad2d	-2	-	0	$s+a_2$	-	a_1s+a_0
ad2v	-1	-	+1	s^2+a_2s	-	$a_1s^2+a_0s$
ad2a	0	-	+2	$s^3+a_2s^2$	-	$a_1s^3+a_0s^2$
av2v	-1	-	0	s^2+a_2s	-	a_1s+a_0
av2a	0	-	+1	$s^3+a_2s^2$	-	$a_1s^2+a_0s$
vd2d	-1	-	0	s^2+a_2s	-	a_1s+a_0
vd2v	0	-	+1	$s^3+a_2s^2$	-	$a_1s^2+a_0s$
avd2d	-2	-1	0	s	$a_2s+ a_1$	a_0
avd2v	-1	0	+1	s^2	$a_2s^2+ a_1s$	a_0s
avd2a	0	+1	+2	s^3	$a_2s^3+ a_1s^2$	a_0s^2

Table II The set of 10 CF elemental 'numerator' pairs $\{B_p, D_p\}$; the 'denominator' pair $\{A, C\}$ is invariant for all CF.

CF name	CF elemental 'numerator' pairs $\{B_p, D_p\}$					
	B_h^T	D_h	B_m^T	D_m	B_l^T	D_l
ad2d	$[0\ \ 1\ \ a_2]$	[0]	-		$[0\ \ a_1\ \ a_0]$	[0]
ad2v	$[1\ \ a_2\ \ 0]$	[0]	-		$[a_1\ \ a_0\ \ 0]$	[0]
ad2a	$[0\ \ -a_1\ \ -a_0]$	[1]	-		$[a_0\text{-}a_1a_2\ \ -a_1^2\ \ -a_1a_0]$	$[a_1]$
av2v	$[1\ \ a_2\ \ 0]$	[0]	-		$[0\ \ a_1\ \ a_0]$	[0]
av2a	$[0\ \ -a_1\ \ -a_0]$	[1]	-		$[a_1\ \ a_0\ \ 0]$	[0]
vd2d	$[1\ \ a_2\ \ 0]$	[0]	-		$[0\ \ a_1\ \ a_0]$	[0]
vd2v	$[0\ \ -a_1\ \ -a_0]$	[1]	-		$[a_1\ \ a_0\ \ 0]$	[0]
avd2d	$[0\ \ 1\ \ 0]$	[0]	$[0\ \ a_2\ \ a_1]$	[0]	$[0\ \ 0\ \ a_0]$	[0]
avd2v	$[1\ \ 0\ \ 0]$	[0]	$[a_2\ \ a_1\ \ 0]$	[0]	$[0\ \ a_0\ \ 0]$	[0]
avd2a	$[-a_2\ \ -a_1\ \ -a_0]$	[1]	$[a_1\text{-}a_2^2\ \ -a_2a_1\ \ -a_2a_0]$	$[a_2]$	$[a_0\ \ 0\ \ 0]$	[0]